ACS NANO

www.acsnano.org

ARTICLE

Observation of Yu–Shiba–Rusinov States and Inelastic Tunneling Spectroscopy for Intramolecule Magnetic Exchange Interaction Energy of Terbium Phthalocyanine (TbPc) Species Adsorbed on Superconductor $NbSe_2$

Syed Mohammad Fakruddin Shahed, Ferdous Ara, Mohammad Ikram Hossain, Keiichi Katoh, Masahiro Yamashita, and Tadahiro Komeda*

Cite This: *ACS Nano* 2022, 16, 7651–7661

Read Online

ACCESS | Metrics & More | Article Recommendations | Supporting Information

ABSTRACT: We investigated the spin properties of the terbium phthalocyanine (TbPc) species adsorbed on the superconductor $NbSe_2$ surface using scanning tunneling microscopy and spectroscopy. $TbPc_2$ is a molecule in a class of single-molecule magnets (SMMs), and the use of superconductor electrodes attracts attention for the application to the devices using the spin degree of freedom. TbPc is a building block of $TbPc_2$ and can reveal the spin component's behavior. In the experiment, TbPc species were placed on the surface of the superconductor $NbSe_2$. We measured Yu–Shiba–Rusinov (YSR) states caused by the interaction between the superconducting state and magnetic impurity and inelastic tunneling spectroscopy (IETS) for the spin excitation, below 1 K. We also measured the Kondo state formed by the magnetic singlet formation. We detected the radical spin at the ligand position of the TbPc by the presence of the Kondo peak and demonstrated that the radical spin forms the YSR feature. In addition, the exchange interaction energy (E_{ex}) between the spins of the radical ligand (Pc) and the center 4f metal atom (Tb^{3+}) is determined by using the IETS technique. E_{ex} is a critical parameter that determines the blocking temperature, below which the sample behaves as an SMM. IETS results show that the statistical distribution of E_{ex} has peaked at 1.3, 1.6, and 1.9 meV. The energy range is comparable to the recent theoretical calculation result. In addition, we show that the energy variation is correlated with the bonding configuration of TbPc.

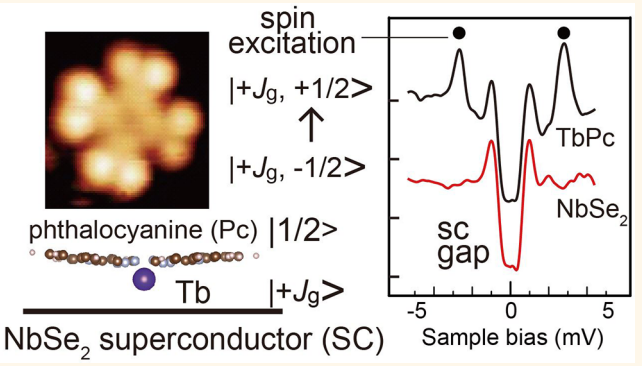

KEYWORDS: *Single-Molecule Magnet (SMM), Exchange Interaction Energy, Terbium Phthalocyanine (TbPc), Superconductor $NbSe_2$, Inelastic Tunneling Spectroscopy, Yu–Shiba–Rusinov States*

Molecule complexes with a 4f lanthanide atom show intriguing properties, including the single-molecule magnet (SMM) behavior. The SMM molecule can maintain the spin direction below a temperature called the blocking temperature (T_B) for a certain period.[1−3] This property makes SMM a promising candidate for the material of devices using the spin degree of freedom, especially the quantum information process.[4−7]

Continuous efforts have been devoted to achieving a higher T_B for the SMM complex after the first finding of the SMM with transition metals. Recently, the exchange interaction between the ligand and the metal ion has attracted attention as a critical parameter to realize a higher T_B. The exchange interaction energy (E_{ex}) is smaller for the 4f metal compared to the transition metals. However, recent reports revealed that a higher T_B could be achieved in the Dy complex when two Dy

Received: December 17, 2021
Accepted: April 21, 2022
Published: April 25, 2022

atoms sandwich an N radical than a simple Dy−N combination. The mechanism has been attributed to the increase of the exchange interaction by making the E_{ex} between the Dy ion and the radical double.[8,9]

In addition, E_{ex} is an essential parameter for the spintronic application of the SMM molecule. A strong coupling between the itinerant electron and a 4f electron is required to read the 4f spin state by the electric current that flows through the molecule. However, the interaction is usually small due to the localized nature of the 4f state. A previous report that detected the 4f spin by the electric current attributed the radical spin of the ligand as an interface of the two.[10] The delocalized ligand π electron can be well-coupled with the conduction electron, and the π electron is connected with the 4f state through the exchange interaction. Thus, the E_{ex} is critical for detecting the 4f spin by the conduction electrons. Despite the importance, the direct detection of the E_{ex} is not accessible due to the selection rule of the experiments using the photons. Several reports examined these parameters for SMM molecules using the inelastic neutron scattering technique.[11,12]

Here, we investigate the TbPc species adsorbed on the superconducting $NbSe_2$ surface using scanning tunneling microscopy/spectroscopy (STM/STS) below the temperature of 1 K. We measured Yu−Shiba−Rusinov (YSR) states, caused by the magnetic interaction between the superconductor and the adsorbate, inelastic tunneling spectroscopy (IETS), which measures the spin-excitation energy, and the Kondo state, formed by the magnetic singlet formation around an isolated spin. The TbPc species is a building block of the SMM complex of bis(phthalocyaninato)terbium(III) ($TbPc_2$). We confirmed the existence of the radical spin at the ligand position of the TbPc by the presence of the Kondo peak. We also demonstrated that the radical spin forms the YSR feature. Though Island and co-workers demonstrated the excitation of the YSR states using the break-junction device, in which a radical molecule is bridging the superconductor electrodes,[13] we believe few studies have reported the YSR state formed by a π radical using an STM setup, providing higher spatial resolution. We successfully detected IETS peaks corresponding to the excitation from the antiparallel to the parallel coupling between the Tb angular momentum and the ligand unpaired π spin. The statistical distribution of E_{ex} has peaked at 1.3, 1.6, and 1.9 meV, comparable to the previous calculation result of 1.0 meV for the $TbPc_2$. In addition, we detected the E_{ex} variation with an atomic-scale position change, which is due to the change of the local bonding configuration of TbPc, implying the possibility of the tuning of the E_{ex} with an intramolecule precision.

RESULTS AND DISCUSSIONS

Structural and Electronic Configuration of TbPc Species. First, we show the STM images of the surface after $TbPc_2$ molecules were deposited on the cleaved surface of the superconductor $NbSe_2$. The substrate image is shown in the inset of Figure 1(a). We observe the 3 × 3 superstructure of the charge density wave (CDW) of the 2H phase.[14−16]

The STM image of a robust double-decker $TbPc_2$ molecule adsorbed on the coinage metal surfaces has been reported with a typical height of 400 pm.[17−19] The height is roughly double that for the single-decker metal−Pc molecules of CoPc and CuPc on those surfaces.[20−23] As shown in Figure 1(a), at least two species appear with different heights. In this panel, the two bright molecules are higher than those of the eight-lobe species

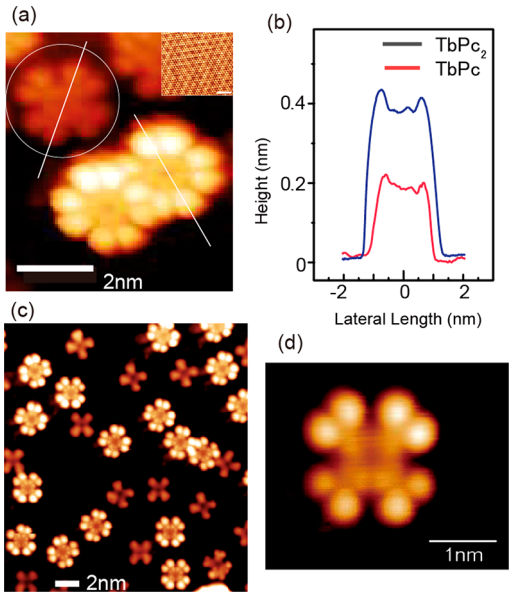

Figure 1. (a) Topographic image of two $TbPc_2$ molecules and one TbPc species (marked by a circle), showing brighter and darker contrast, respectively. (V_s = −800 mV, I_t = 0.1 nA, scale bar = 20 nm) An atomic-scale image of the cleaved $NbSe_2$ surface is shown in the inset (scale bar = 2 nm). (b) Cross-sectional height profile of the $TbPc_2$ and TbPc observed in (a). (c) Mixed species of TbPc and Pc appeared as eight-lobe and cross-shaped moieties, respectively. (d) Close-up view of TbPc molecule (scale bar = 2 nm).

marked with a circle. We compare the heights of those two in the cross-sectional height profile shown in Figure 1(b). The 200 and 400 pm species are dissociated and robust species of $TbPc_2$, respectively. We observed species with the height of 200 pm when the $TbPc_2$ molecules were deposited on reactive metal surfaces like Ni and Co, which work as catalysts for the dissociation of the $TbPc_2$ molecule. For these metal surfaces, the dissociation was suppressed by cooling the substrate below the liquid N_2 temperature during the deposition. However, there always appears robust and dissociated $TbPc_2$ on the $NbSe_2$ surface.

When a $TbPc_2$ molecule is dissociated, we expect both TbPc and Pc species. We can observe both species on the same substrate area, shown in Figure 1(c). There are two groups among the ∼200 pm species categorized by the STM images: a cross and an eight-lobe shape. The former cross-type is commonly observed for the single-decker metal−Pc molecules, including the H_2Pc molecule on Au(111),[24] and we attribute it to the Pc species. On the other hand, we should assign the eight-lobe species to TbPc. The magnified image of the TbPc species is shown in Figure 1(d), in which we see the center part is lower in height than the ligand part.

Hereafter, we focus on the TbPc species and observe the spectroscopy features of (1) the states newly formed by the interaction between the superconductor and molecule spin and (2) the intramolecule exchange interaction between the spins of the Tb atom and the Pc ligand. In the robust $TbPc_2$ molecule, the Pc ligands cover the center Tb atom on both sides. Thus, the delocalized molecule orbital of the Pc ligand screens the 4f spin feature, making detection difficult. We consider the TbPc species appropriate for detecting the Tb spin information, in which the Tb ion is exposed to one side of the species.

https://doi.org/10.1021/acsnano.1c11221
ACS Nano 2022, 16, 7651−7661

We consider the structural and electronic configurations of the TbPc species. We first use a model in which a $TbPc_2$ molecule is placed in the vacuum, the ionic state of Tb is 3+, and the two Pc ligands show the mixture of the 2− and 1− states (see Figure 2(a)).[25] The Pc with the 1− ionic state is a radical ligand and possesses a spin from the unpaired π orbital.

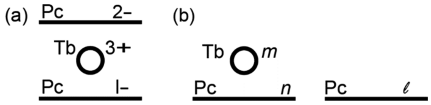

Figure 2. Ionic states of the robust $TbPc_2$ (a) and two species after dissociation to TbPc and Pc (b). Oxidation numbers are depicted at each element.

We can reproduce such behavior by the Vienna Ab initio Simulation Package (VASP) calculation, in which the 4f electrons are treated as the core electrons with the ionic state of 3+, and the spin polarization is included. After the structural optimization, the total energy of $E(TbPc_2)$ and the spin polarization of the π orbital are calculated. We then separated the model molecule into two species, as illustrated in Figure 2(b). As a result of electron transfer in the dissociation, several kinds of ionic states appear in the two species. The oxidation numbers of the two Pc are defined as n and l. Since the Pc started from a neutral condition, these two should satisfy the relation of $n + l = -3$, since the assumption of $m = +3$ is rational. We calculated the spin polarization and the total energy of TbPc for $n = -3$, -2, and -1 and those for Pc of the corresponding oxidation states of $l = 0$, -1, and -2. In the calculation, we specified the number of electrons in each species by setting the calculation parameter of the VASP.

The spin polarization of TbPc is 0.4 μ_B, 0 μ_B, and 0.8 μ_B for $n = -3$, -2, and -1, respectively. Thus, the TbPc is spin-polarized for $n = -3$ and -1, the latter of which shows an identical spin polarization as was calculated for the $TbPc_2$.[19]

In addition, the energy of $E(TbPc) + E(Pc) - E(TbPc_2)$ can be scaled with the dissociation energy for each ionic state and the probability of finding it on the surface. The estimated difference between the three oxidations states is negligible. Thus, we may observe all of these species on the surface. However, if we select the species with the most robust spin feature, we can choose the TbPc species with the Pc's oxidation state of −1. Using this method, we can access the E_{ex} for the robust $TbPc_2$.

Kondo Resonance. We now examine the presence of the magnetic moment in the molecule experimentally. We employ the Kondo resonance for the detection of the spin. The Kondo state is formed at the position of the molecule's spin and shows a large density of states,[26,27] observed in single atoms[28−33] and single molecules.[19,34−44] We previously examined the Kondo state for the $TbPc_2$ molecule adsorbed on the Au(111) surface[19] and found a sharp Kondo peak in the STS at the lobe position originating from the unpaired π orbital. However, we found no Kondo feature at the center, which is due to the localized nature of the 4f spin, making the detection of the itinerant electron difficult.

We measured the STS on the TbPc species at 11 K, above the critical transition temperature (T_c) of $NbSe_2$. Setting the temperature above T_c can diminish the interference between the Kondo resonance and the Cooper pair of the superconducting state. The results are illustrated in Figure 3, in which we see an enhanced Kondo peak at the lobe position. In addition, a clear peak is observed at the center, which is missing in the spectrum obtained on the Au(111) surface.

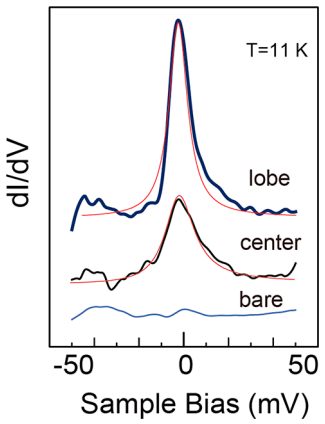

Figure 3. Kondo features observed for TbPc species on $NbSe_2$ at the positions of lobe and center at the sample temperature of 11 K. The bare $NbSe_2$ spectrum is shown for comparison. Thin red lines correspond to the fitted results with the Fano formula (see text).

We analyze the Kondo features with the Fano function, whose detail is in section 1 of the SI. The half widths were 7.4 and 9.2 meV at the lobe and the center, respectively. They correspond to 81 and 106 K Kondo temperatures, the former of which is slightly higher than that of $TbPc_2$/Au(111) but belongs to a class of weak interaction between the TbPc and $NbSe_2$ substrate.

The observation of the Kondo feature at the center of the lanthanide double-decker Pc molecule was reported in several cases. For the $DyPc_2$ molecule adsorbed on Cu(100),[45] the origin of the Kondo feature at the molecule's center was explained by the mixing between the f and d states of the Dy atom, which further contributes to the coupling between 4f and the π electron. More recently, Bucher and co-workers demonstrated that the $TbPc_2$ molecule shows the Kondo peak at the molecule's center position when adsorbed on the Cu(111) surface,[46] which is attributed to the significant rearrangement of the electron with the strong interaction between the molecule and the substrate. The Kondo feature of TbPc at the center should be due to the change of the Tb's d and f orbitals by the direct interaction with the substrate. The mixture of d and f orbitals makes the 4f spin-coupled with the π state to form the Kondo state.

We illustrate the STS for the broader energy region in Figure S1 of the SI. We previously reported the STS spectra for the $TbPc_2$ molecule adsorbed on the Au(111) surface.[47] By comparing these results, we judge that the STS spectrum of TbPc species exhibits a feature originating from the singly occupied molecular orbital (SOMO), in addition to the highest occupied molecular orbital (HOMO) and lowest unoccupied molecular orbital (LUMO). The appearance of the SOMO state supports the existence of the unpaired π orbital, the origin of the Kondo feature we showed above.

Observation of Yu−Shiba−Rusinov (YSR) States. We can obtain further evidence of the magnetization of the TbPc species by detecting the Yu−Shiba−Rusinov (YSR) state.[48] In the STS spectrum, the YSR state appears within the SC gap. For the spherical symmetric exchange interaction potential between the magnetic impurity and the superconductor, it can be simplified and expressed with the following formula

https://doi.org/10.1021/acsnano.1c11221
ACS Nano 2022, 16, 7651−7661

$$\epsilon_0 = \frac{E_0}{\Delta_0} = \frac{1 - (J_0 S\pi N_0/2)^2}{1 + (J_0 S\pi N_0/2)^2} \quad (1)$$

where E_0 is the bound-state energy, Δ_0 is the order parameter, J_0 is the exchange interaction energy, S is the impurity spin, and N_0 is the density of state of the normal state.[49] Flatté and co-workers estimated such energy positions, which represent the local pair breaking excitation, as a function of the magnetic exchange potential.[50] As the potential strength increases, the peak position of the YSR state moves toward the Fermi level. More recent reports show that the energy position is susceptible to the minute change of the exchange interaction of the impurity interacting with the substrate.[51,52]

The behavior of YSR peaks in the STS was reported for magnetic atoms like Co[51] and Fe[53] and magnetic molecules.[54−59] Especially, much attention is paid to the phthalocyanine monomer and dimers.[56−58] Despite such previous works, both $TbPc_2$ and TbPc have unique properties, which are missing in the above cases and rationalize further investigation. First, they have two types of spins in each species: an unpaired delocalized π orbital plus a 4f spin of Tb atom. Since fewer studies reported that the YSR state originated from π orbital, the study of the YSR states for these species is significant. Second, there is a rising interest in applying SMM $TbPc_2$ to the device using the spin degree of freedom. It is critical to understand how the electrode disturbs the spin condition of $TbPc_2$ in order to maintain the information on the spin direction. The use of the superconductor surface is intriguing, for the control of the spectroscopic information is necessary.

We compare the YSR features for $TbPc_2$ and TbPc species, which appear in the same surface area (see Figure 4(a)). For

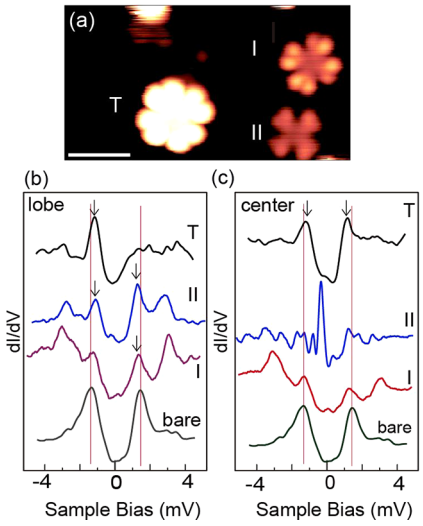

Figure 4. (a) Topographic image of types I and II of TbPc and $TbPc_2$ molecules, marked by I, II, and T, respectively. (b,c) YSR features obtained at the lobe (b) and the center (c) of the species.

the TbPc species, the typical one shown in Figure 1 is depicted as the type I species. TbPc species with slightly less height are named type II, which appear with a more negligible probability (less than 10%). We can easily distinguish type II and pure Pc species from their size and shape.

At the lobe position for all three species, we observe the features inside the superconductor gap (see Figure 4(b)). They are separated 0.25 meV from the superconductor edge. The lobe of $TbPc_2$ shows a strong asymmetry in the intensity of the right and left features. A similar asymmetry was reported for the MnPc molecule on Pb(111).[52] The appearance of the asymmetric shape in the excitation peaks reflects the breaking of the time-reversal symmetry by the magnetic interaction between the Cooper pairs and the spin of the π orbital of $TbPc_2$.[49,60] The lobe-position spectrum shows little difference between type I and type II. We will focus on the part outside of the SC gap later. However, when observed at the center (Figure 4(c)), there appears a significant difference between the type I and type II species. The one for type II shows a vital YSR feature compared to type I. We consider this difference is deduced by a change in the binding site of the TbPc species. As shown in the Figure S2 of SI, the center position changes from the on-top site of type I to the hollow site for type II. The latter can make a stronger bonding between Tb and Se layers compared to the former, which causes the lower height of the species. As a result, the exchange interaction J in eq 1 increases, followed by more significant energy separation from the SC gap. The YSR peak appears close to the Fermi level for type II. It demonstrates that the property of the YSR feature for the Tb atom is sensitive to the bonding configuration. Wang and co-workers demonstrated that the change of the adsorption symmetry of CoPc on the $NbSe_2$ surface drastically changes the YSR features in the STS spectrum originating from the absence of the inversion symmetry of the 2H phase $NbSe_2$.[61] We need a further calculation study of the 4f state of TbPc regarding the appearance/disappearance of the YSR feature for TbPc.

TbPc Component with Tb-Up and Tb-Down Configurations. The Pc molecules centered by diatomic moieties like VO,[62−64] TiO,[65] SnO,[66] and ClAl[67] and simple metal atoms of Sn[66,68,69] and Pb[70] have nonplanar structures. The nonplanar configuration is due to the large ion radius of the center species, in which Sn and Pb ions have a radius larger than 1 Å. It cannot fit in the center of the Pc moiety when the ion radius becomes more extensive. The ion radius of Tb^{3+} is larger than 1 Å and is expected to have a nonplanar structure. It is debated whether the center part is directed to the vacuum or the surface for these nonplanar Pc complexes.

To examine this issue for the TbPc case, we produced simulation images of the STM using VASP. We optimized the adsorption configuration by considering the vdW interaction. For the starting bonding structure, we placed the TbPc species so that the center Tb atom is aligned with the on-top site of the Se atom and one of the symmetry lines of the TbPc is aligned to (−110) direction. This model is based on the STM image of TbPc species of atomic resolution (see Figure S2(a) in the SI). The optimized structures are shown in Figures S2(c,d) for the Tb-down and Tb-up species, respectively. After calculating the electronic structure, we computed the STM images using a previously reported method,[71] based on the Tersoff and Hamman theory.[72]

We simulated images of the TbPc species with the $n = -1$ state; Tb-down and Tb-up configurations are shown in Figure 5(a,b), respectively. The center is darker (brighter) than the ligand part for Tb-down (up) configurations. Several reports compared the simulation images and the STM topographic images for the SnPc, where the center part appears darker (brighter) than the Pc ligand for Sn-down (Sn-up).[66,68,69] By comparing with the TbPc topographic image shown in Figure 5(c), we judged that the majority of the TbPc species adsorbs

https://doi.org/10.1021/acsnano.1c11221
ACS Nano 2022, 16, 7651−7661

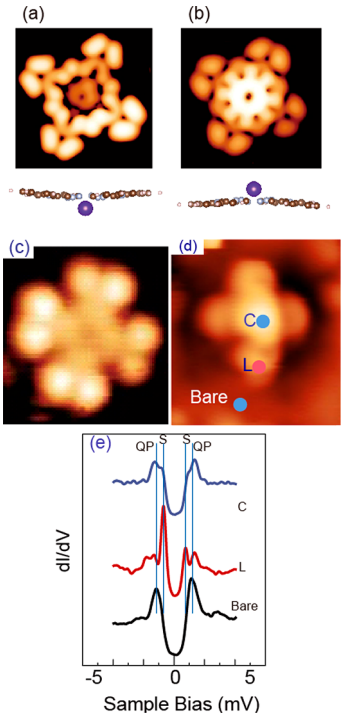

Figure 5. (a,b) STM simulation images forrmed by the VASP calculation for Tb-down (a) and Tb-up (b) TbPc species, together with the side-view model. (c,d) Correspondting STM images for Tb-down (c) and Tb-up (d) cases. (e) STS spectra obtained at the positions specified in (d). Vertical lines indicate QP and YSR features (see main text).

with the Tb-down configuration, since the center of the image appears lower in *z*-height. However, we also observed a species where the center part is enhanced with a tiny probability of 1%, whose image is shown in Figure 5(d). The structure corresponds to the Tb-up bonding configuration, judging from the similarity with the simulation image of Figure 5(b).

When the TiO[64] and Sn[66,68,69] are pointing down, the bonding to the surface is less stable than in the case of pointing up. The former is like standing with a single leg on the surface, tilted or dragged by the STM tip. A similar phenomenon appears in our system, which we will describe later.

We illustrate STS for the Tb-up species in Figure 5(e), whose measurement positions are specified in Figure 5(d). The energy position of the quasiparticle at the bare part of the surface (marked "Bare") is shown by straight lines with mark "QP". For the spectrum at the lobe position (marked "L"), we see a clear YSR peak separated 0.51 meV from the QP position with asymmetric intensities for the positive and negative bias features. The QP position's split energy is almost twice that for the Tb-down case, which indicates a more vital interaction between the π radical spin and the substrate. The shorter distance between these two should be the reason. The spectrum obtained at the center (mark C) also shows the YSR feature, which appeared at the same energy position of the lobe spectrum with less intensity. The YSR state behavior is different from the reported CoPc on the $NbSe_2$ surface, in which the YSR state is most separated from the superconductor edge toward the Fermi level and gradually approaches the gap edge with the move of the tip to the perimeter of the ligand.[57] The YSR feature of the center of the Tb-up TbPc species should be originated from the delocalized π orbital spin instead of the 4*f* spin. The difference is mainly due to the lifted position of the Tb atom from the $NbSe_2$ surface.

Inelastic Tunneling Spectroscopy for the Exchange Interaction Energy. We now show the tunneling spectroscopy obtained for the TbPc species with the Pc^{1-} oxidation state in Figure 6(a), intended to obtain the exchange interaction energy. We superimpose the spectrum of the $NbSe_2$ by the red line as a reference spectrum. For the pristine surface, we can identify the superconductor gap flanked by two quasiparticle peaks positioned at the energies of ±1.3 meV. For the STS obtained on the lobe position of the TbPc species, we identify additional features at the symmetric positions of ±2.9 meV marked by IE_R and IE_L. In the tunneling spectroscopy, features that appear at the symmetric positions around the Fermi level are often assigned to the inelastic tunneling process.

The tunneling electron causes an elementary excitation during the tunneling process (energy defined as $\hbar\omega$).[73,74] Applying the IETS technique to the superconducting substrate can generate higher-resolution spectroscopy due to the sharp width of the excitation feature of the superconductor.[58,75−78] For the SMM molecule, Burgess and co-workers investigated the intramolecule exchange interaction among the metal atoms of Fe_4 SMM molecule.[77] Our study focuses on the metal−ligand exchange interaction, which is correlated with the blocking temperature of SMM. We illustrate the relation between the energy position of the inelastic tunneling feature and the excitation energy in Figure S3 of the SI. Briefly, the

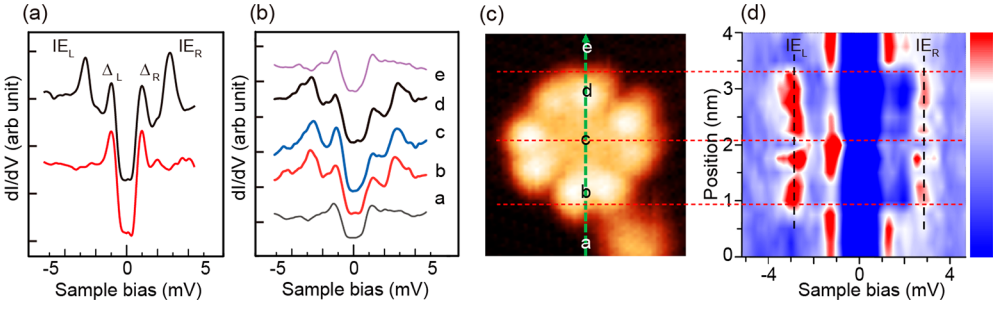

Figure 6. (a) Comparison of STS near the Fermi level obtained at the pristine $NbSe_2$ and the lobe position of the TbPc species shown in Figure 1(d). (b) Position-dependent variation of the STS spectra, whose positions are specified along a vertical line in the topo image of (c). (d) Color map of the STS variation. The horizontal axis is the bias energy, and the vertical axis represents the positions along the vertical line of (c). The intensity of the STS spectra is depicted with the color variation shown in the color table.

https://doi.org/10.1021/acsnano.1c11221
ACS Nano 2022, 16, 7651−7661

inelastic peaks appear at $\pm(\Delta + \hbar\omega)$, in which Δ indicates the elastic excitation energy related to the superconductor state.

The peaks marked by IE_L and IE_R in Figure 6(a), outside of the superconductor peaks of Δ_L and Δ_R, correspond to the inelastic tunneling peaks. In addition, we examined the spectrum variation due to the tip position change in Figure 6(b). The tip positions are indicated in the topo image of Figure 6(c) with the marks a−e. The variation of the spectra is further visualized in the color mapping in Figure 6(d), in which the *x*-axis is the sample bias, and the *y*-axis is the tip position along the vertical line of Figure 6(c). The dotted horizontal line shows the correspondence of Figure 6(c,d). The conductance amplitude is expressed in the color that varies according to the color table shown on the right-hand side of Figure 6(d).

The QP peaks at ±1.3 meV are visible in Figure 6(d) as enhanced features, which quickly weaken when the tip moves to the lobe positions of b and d. The IE features at ±2.9 meV are enhanced at these positions. At position c, near the center of the TbPc species (Tb position), the QP peaks returned to the intensity of that observed out of the molecule. The spatial distribution of the IE peaks is similar to that of the π orbital of the Pc ligand.

However, we have to distinguish whether this excitation is originated from vibration-related or spin-related excitation. There are several vibrational modes in this energy range, including the Pc ligand's breezing mode and hindered translational mode along the surface. To judge whether the peak originated from the phonon and the spin excitation, we have to apply a magnetic field that can lift the degenerated spin multiples. However, we have to note that, different from the metal surface, the electronic state of the superconductor surface changes with the magnetic field application; the SC gap might collapse with the applied magnetic field, and the sharpness of the final state will be much affected.

We show the variation of the STS spectrum with the application of the magnetic field B obtained at the positions of the center and the lobe of the TbPc species. We see the IETS peaks marked by IE_L and IE_R become less apparent with B due to the collapse of the superconducting state with the magnetic field. The spectrum change with B observed at the substrate part is shown in Figure 7(c). We can identify an intriguing split of IE_L and IE_R with B despite the shape changes. For that purpose, we repeated the B cycle more than 10 times and improved the signal-to-noise ratio. The breaks of the IE_L state with B at the center and the lobe positions are illustrated in Figures 7(d,e), respectively, with two eye-guide lines. The statistical summary of the magnitude of the energy split is then plotted in Figure 7(f) with the linear fitting result, which shows a slope of 235 μV/T. The error bars are calculated from the deviation from cycle to cycle. The separation of the IE_L and IE_R with the B application indicates that the peak is derived from the spin excitation.

We consider the spin-excitation energy and the origin of the peak split by the outer magnetic field, B. The total Hamiltonian in the presence of the external magnetic field can be expressed like the following[11]

$$\hat{H}^{\text{eff}} = \hat{H}^{\text{Tb}}_{\text{LF}} + J_{\text{ex}}\hat{S}^{\text{Pc}}\cdot\hat{J}^{\text{Tb}} + \hat{H}^{\text{Tb}}_{\text{Zeeman}} + \hat{H}^{\text{Pc}}_{\text{Zeeman}} \quad (2)$$

The term $\hat{H}^{\text{Tb}}_{\text{LF}}$ represents the ligand-field split among the substates of $J = 6$. For the $TbPc_2$ molecule, $J_z = \pm 6$ is assigned to the ground state. The energy difference between ±6 and ±5 is calculated to be larger than 70 meV.[79] However, it is not clear whether this energy relation is conserved for the TbPc species, since it was reported that $J_z = \pm 5$ is the ground state for some Tb complexes: for example, the polyoxometalate (POM)-based double-decker lanthanide complex $[LnP_5W_{30}O_{110}]^{12-}$ (Ln^{3+} = Tb, Dy, Ho, Er, Tm, and Yb)[80] and, more recently, the $[M^{III}(Pc)(PW_{11}O_{39})]^{6-}$ (M = Y, Dy, Tb) double-decker.[80]

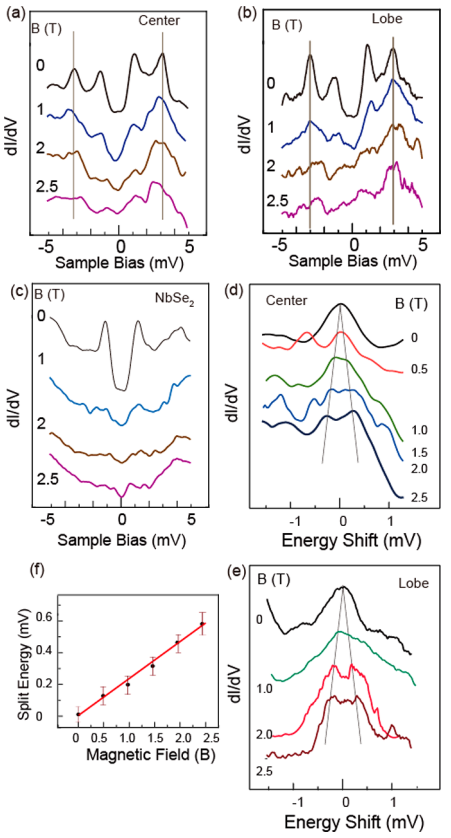

Figure 7. Variations of STS with an application of B. The tip position on the center (a) and on the lobe position (b) of the TbPc species shown in Figure 1(d). (c) Reference-B-dependent STS on the $NbSe_2$ surface. (d,e) Magnified plot focusing on the split of the inelastic excitation feature with the B application for the center (d) and the lobe (e). (f) Summary of the split energy vs B.

The term of $J_{\text{ex}}\hat{S}^{\text{Pc}}\cdot\hat{J}^{\text{Tb}}$ corresponds to the intramolecule E_{ex} between the π radical of the Pc ligand (spin 1/2) and the angular momentum of the Tb atom expressed with the quantum number of $\hat{J}^{\text{Tb}}$. Pederson and co-workers reported a theoretical calculation that estimates the E_{ex} for the $TbPc_2$ molecule. In such a case, the antiparallel orientation of the Tb angular momentum and the Pc ligand spin is calculated to be more stable than the parallel one through the exchange interaction.[81] Their numerical estimation should represent J_{ex} and $J_{\text{ex}}\hat{S}^{\text{Pc}}\cdot\hat{J}^{\text{Tb}}$ as 0.1 and 1.01 meV, respectively. A more recent calculation taking into the spin-polarization effect of the π system was reported by Huang et al.,[82] in which the authors claim to have produced the same result. The inelastic excitation energy estimated in our experiment was slightly larger than the value of 1.01 meV but in the close range. As stated above, there is a possibility that the ground state for TbPc is not $J_z = \pm 6$. However, we consider that the effect of J_z variation for the total E_{ex} is small.

https://doi.org/10.1021/acsnano.1c11221
ACS Nano 2022, 16, 7651−7661

$\hat{H}^{Tb}_{Zeeman} + \hat{H}^{Pc}_{Zeeman}$ corresponds to the Zeeman energy when an external magnetic field is applied. We can explain the mechanism of the split of the excitation peak and its amplitude more easily with the graphical diagram shown in Figure 8. In

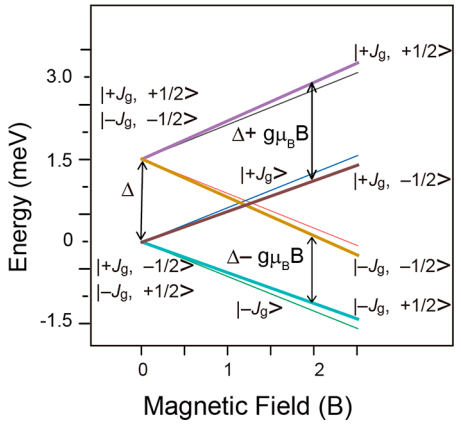

Figure 8. Energy diagram of the exchange interaction between the combined state of the Tb angular momentum and the spin of the radical ligand and the Zeeman effect with an applied magnetic field B.

the figure, antiparallel alignment between the Tb angular momentum and the ligand π radical spin is expressed as a more energetically stable state than that of the parallel one,[81] whose energy splits are represented as 1.5 meV based on the result of this experiment. The combination of the angular momentum and the spin state of Tb and the Pc radical ligand is expressed as $|J_z, s_z>$. We consider the ground state of the system. Due to the ambiguity of the ground state for the angular momentum, we express it as $\pm J_g$ ($J_g > 0$). Thus, the following four cases are considered: $|\pm J_g, \pm 1/2>$.

The pair of $|-J_g, +1/2>$ and $|+J_g, -1/2>$ is energetically more stable than the other pair of $|+J_g, +1/2>$ and $|-J_g, -1/2>$. The energies of each pair degenerate at the $B = 0$ condition. The excitation energy detected in our experiment should correspond to $|-J_g, +1/2> \rightarrow |-J_g, -1/2>$ and $|+J_g, -1/2> \rightarrow |+J_g, +1/2>$.

Although the energy positions of both the Tb angular momentum state and the radical spin state shift with the application of B, the change of the excitation energy is derived only from the radical part. As illustrated in Figure 8, the energy of the excitation for $|-J_g, +1/2> \rightarrow |-J_g, -1/2>$ and $|+J_g, -1/2> \rightarrow |+J_g, +1/2>$ will decrease and increase with B application, respectively. Then, the two excitation paths do not degenerate anymore and should show a split state, whose energy difference is $2g_e\mu_B B$, where g_e and μ_B correspond to the g factor for the spin 1/2 system and the Bohr magnetron, respectively. In a numerical estimation, the energy split is given by 232 μeV/B and shows a good coincidence with the slope given above.

Bonding Configuration and Intramolecule Exchange Interaction Variation. We discuss a statistical distribution of E_{ex}. For this purpose, we measured the inelastic excitation at the lobe positions of more than 100 molecules and made a histogram of Figure 9(a). We omitted lobes for which the inelastic peak was absent in the counting. We can fit the distribution with three Gaussian distributions and illustrate the fit results by the solid curve. The energies of the center position are 1.3, 1.6, and 1.9 meV, which we named E1, E2,

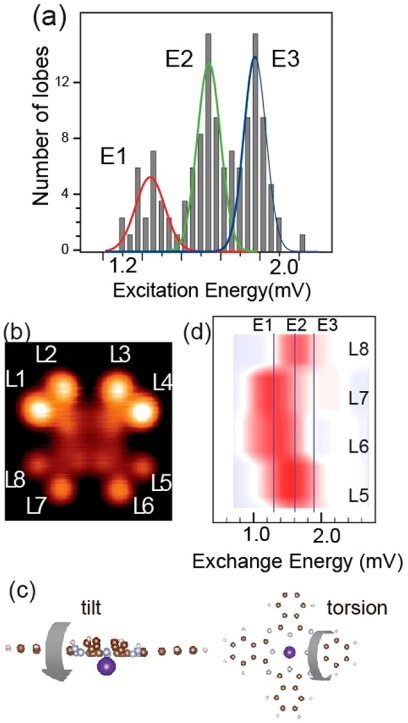

Figure 9. (a) Histogram of exchange interaction energy after the excitation energies observed for more than 100 lobes of TbPc species are summarized. (b) Topo images of TbPc. Ligand lobes L1−L8 are marked. (c) Illustration of the tilt and torsion of the species as a possible origin of the contrast variation. (d) Position-dependent exchange interaction energy variation expressed with color mapping; the *x*-axis is the energy, and the *y*-axis is the lobe position for the TbPc of (b).

and E3, respectively. We consider that the discrete three groups of the E_{ex} should be derived from the bonding configuration together with the intrastructure change of TbPc.

First, we check the asymmetric topo image of Figure 9(b). The lobe pairs (L1, L2) and (L3, L4) appear higher than those of (L5, L6) and (L7, L8), which are due to the canted configuration. The tilt of the TbPc is depicted in Figure 9(c), for which the bonding should cause a single Tb atom attached to the Se atom. In addition, among the dark lobe groups, L5 and L8 are further lower than the L6 and L7, derived from the indole's torsion effect, shown in Figure 9(c).

The lobes of L5−L8 show clear inelastic peaks. We illustrate E_{ex} variation with the color mapping in Figure 9(d), where the red corresponds to the region of high intensity in IETS. E_{ex} is higher for L5 and L8 than L6 and L7. The former and the latter correspond to E2 and E1. We can simply understand that the part of the molecular orbital with a smaller distance to the $NbSe_2$ substrate exhibits a larger E_{ex}. Boukhvalov and co-workers showed that the intramolecule exchange interaction changes with the ligand substitution, which is explained by the charge distribution in the ligand and the metal−ligand hybridization.[83] Similarly, the tilt and torsion of the molecule make an uneven interaction between the indole and the substrate in a local manner, which changes the charge distribution and E_{ex}. The important part is that such a site-dependent difference of the ligand−substrate interaction appears as an STS variation with an atomic-scale resolution. We reported a similar phenomenon for $TbPc_2$/Au(111) system. When the Pc ligand is tilted, the Kondo feature from

https://doi.org/10.1021/acsnano.1c11221
ACS Nano 2022, 16, 7651−7661

the π radical spin shows the variation of the peak width and the intensity with the atomic-scale resolution.[47] Similarly, E_{ex} shows atomic-scale intraspecies variation with the nonuniform interaction with the substrate.

CONCLUSION

We investigated the spin property of the TbPc species, a building block of SMM, $TbPc_2$, by combining the observation of the Kondo resonance, YSR states, and IETS spectra. Combining STM topo images and DFT calculation, we assigned the majority of the TbPc species adsorbed with the Tb-down configuration, in which the π radical spin remains on the ligand. The unpaired spin on the delocalized π orbital was confirmed experimentally by observing the Kondo resonance on the ligand at 11 K. We observed that the same spin produces a YSR feature, which is one of few reports of the YSR feature formed by a spin of the delocalized orbital. The YSR features show an intriguing variation with bonding configuration. The STS obtained at the center of the Tb-down TbPc shows an enhanced YSR peak close to the Fermi level for the case in which Tb is aligned at the hollow site of the Se surface (type II TbPc), which is absent for the on-top configuration.

The IETS measurement revealed the intramolecule exchange interaction energy (E_{ex}) between the Tb atom and the radical Pc ligand of TbPc species. We fit the statistical distribution of E_{ex} analyzed from more than 100 molecules with a Gaussian distribution, which shows three peaks with center energies of 1.3, 1.6, and 1.9 meV. The energy range is comparable to the value of 1.0 meV deduced by a recent theoretical calculation. The corresponding inelastic peaks in IETS spectra show an energy split with applying the outer magnetic field B. The energy split with B supports the assignment of the inelastic peaks to the spin-excitation feature of the antiparallel to parallel alignment of the Tb angular momentum and the radical Pc spin. The variation of E_{ex} is correlated with the change of the bonding configuration. Asymmetric bonding configuration forms atomic-scale local charge rearrangement, which causes the spatial variation of the exchange interaction energy, implying the possibility of tuning such interaction with atomic-scale precision.

METHODS

The substrate $NbSe_2$ surface was prepared by cleaving the bulk crystal in the vacuum condition to expose a mirror-like surface. The molecule of $TbPc_2$ was synthesized by our group and was transferred onto the cleaved $NbSe_2$ surface by the vacuum sublimation method, during which we kept the sample temperature below 50 K. We employed STM and STS, which work at the sample temperature of 400 mK (Unisoku, Japan). A magnetic field up to 10 T can be applied in the surface normal direction. The dI/dV spectra were measured using the lock-in amplifier technique by superimposing the modulation voltage of 50 μV rms onto the tunneling voltage.

The first-principle calculations were performed using the VASP code, employing a plane-wave basis set and projector augmented-wave (PAW) potentials to describe the valence electron behavior.[84,85] A generalized gradient approximation (GGA) was employed using the Perdew–Burke–Ernzerhof (PBE) exchange-correlation potential.[86] The kinetic energy cutoff for the plane-wave basis was set at 400 eV. The positions of the atoms in the TbPc and the top two-unit layers of the $NbSe_2$ slab were optimized without any constraint until the force on individual atoms became less than 0.02 eV/Å. W used the VESTA application. The positions of the atoms in the TbPc species and the top two layers of the $NbSe_2$ slab were optimized without any constraint until the force on individual atoms became less than 0.02 eV/Å. All calculations were done with a spin-polarization activated. We used the VESTA application for visualizing the models.[8787]

ASSOCIATED CONTENT

Supporting Information

The Supporting Information is available free of charge at https://pubs.acs.org/doi/10.1021/acsnano.1c11221.

Fitting of the Kondo feature with the Fano function for the deduction of the Kondo temperature; STS of TbPc on $NbSe_2$; STM images and atom-scale registration of the bonding position of types I and II of TbPc; Energy diagram and energy positions of the peaks in the inelastic tunneling spectroscopy (PDF)

AUTHOR INFORMATION

Corresponding Author

Tadahiro Komeda – *Institute of Multidisciplinary Research for Advanced Materials (IMRAM, Tagen), Tohoku University, Sendai 9800877, Japan;* orcid.org/0000-0003-2342-8184; Email: tadahiro.komeda.a1@tohoku.ac.jp

Authors

Syed Mohammad Fakruddin Shahed – *Institute of Multidisciplinary Research for Advanced Materials (IMRAM, Tagen), Tohoku University, Sendai 9800877, Japan;* orcid.org/0000-0001-6898-6556

Ferdous Ara – *Institute of Multidisciplinary Research for Advanced Materials (IMRAM, Tagen), Tohoku University, Sendai 9800877, Japan*

Mohammad Ikram Hossain – *Institute of Multidisciplinary Research for Advanced Materials (IMRAM, Tagen), Tohoku University, Sendai 9800877, Japan*

Keiichi Katoh – *Department of Chemistry, Graduate School of Science, Josai University, Sakado, Saitama 350-0295, Japan;* orcid.org/0000-0002-0140-8222

Masahiro Yamashita – *Department of Chemistry, Graduate School of Science, Tohoku University, Sendai 980-8578, Japan; School of Materials Science and Engineering, Nankai University, Tianjin 300350, China*

Complete contact information is available at: https://pubs.acs.org/10.1021/acsnano.1c11221

Author Contributions

All authors contributed equally to this work.

Notes

The authors declare no competing financial interest.

ACKNOWLEDGMENTS

We thank Prof. Yasutaka Kitagawa of Osaka University for valuable comments concerning the exchange interaction energy calculation. This study was supported in part by a Grant-in-Aid for Scientific Research (S) (No.19H05621) (Tadahiro Komeda), (C) (No.21K04873) (Syed Mohammad Fakruddin Shahed), and CSRN, Tohoku University. M. Yamashita thanks the support from the 111 project (B18030) from China.

REFERENCES

(1) Woodruff, D. N.; Winpenny, R. E. P.; Layfield, R. A. Lanthanide Single-Molecule Magnets. *Chem. Rev.* **2013**, *113*, 5110–5148.

(2) Liddle, S. T.; van Slageren, J. Improving f-element single molecule magnets. *Chem. Soc. Rev.* **2015**, *44*, 6655−6669.
(3) Sessoli, R.; Powell, A. K. Strategies towards single molecule magnets based on lanthanide ions. *Coord. Chem. Rev.* **2009**, *253*, 2328−2341.
(4) Ungur, L.; Lin, S.-Y.; Tang, J.; Chibotaru, L. F. Single-molecule toroics in Ising-type lanthanide molecular clusters. *Chem. Soc. Rev.* **2014**, *43*, 6894−6905.
(5) Sharples, J. W.; Collison, D.; McInnes, E. J. L.; Schnack, J.; Palacios, E.; Evangelisti, M. Quantum signatures of a molecular nanomagnet in direct magnetocaloric measurements. *Nat. Commun.* **2014**, *5*, 5321.
(6) Shiddiq, M.; Komijani, D.; Duan, Y.; Gaita-Ariño, A.; Coronado, E.; Hill, S. Enhancing coherence in molecular spin qubits via atomic clock transitions. *Nature* **2016**, *531*, 348−351.
(7) Tang, J.; Hewitt, I.; Madhu, N. T.; Chastanet, G.; Wernsdorfer, W.; Anson, C. E.; Benelli, C.; Sessoli, R.; Powell, A. K. Dysprosium Triangles Showing Single-Molecule Magnet Behavior of Thermally Excited Spin States. *Angew. Chem., Int. Ed.* **2006**, *45*, 1729−1733.
(8) Rinehart, J. D.; Fang, M.; Evans, W. J.; Long, J. R. A N23− Radical-Bridged Terbium Complex Exhibiting Magnetic Hysteresis at 14 K. *J. Am. Chem. Soc.* **2011**, *133*, 14236−14239.
(9) Chen, Y.-C.; Liu, J.-L.; Ungur, L.; Liu, J.; Li, Q.-W.; Wang, L.-F.; Ni, Z.-P.; Chibotaru, L. F.; Chen, X.-M.; Tong, M.-L. Symmetry-Supported Magnetic Blocking at 20 K in Pentagonal Bipyramidal Dy(III) Single-Ion Magnets. *J. Am. Chem. Soc.* **2016**, *138*, 2829−2837.
(10) Bogani, L.; Wernsdorfer, W. Molecular spintronics using single-molecule magnets. *Nat. Mater.* **2008**, *7*, 179−186.
(11) Komijani, D.; Ghirri, A.; Bonizzoni, C.; Klyatskaya, S.; Moreno-Pineda, E.; Ruben, M.; Soncini, A.; Affronte, M.; Hill, S. Radical-lanthanide ferromagnetic interaction in a T bIII bis-phthalocyaninato complex. *Phys. Rev. Mater.* **2018**, *2*, 024405.
(12) Baker, M. L.; Tanaka, T.; Murakami, R.; Ohira-Kawamura, S.; Nakajima, K.; Ishida, T.; Nojiri, H. Relationship between Torsion and Anisotropic Exchange Coupling in a TbIII-Radical-Based Single-Molecule Magnet. *Inorg. Chem.* **2015**, *54*, 5732−5738.
(13) Island, J. O.; Gaudenzi, R.; De Bruijckere, J.; Burzurí, E.; Franco, C.; Mas-Torrent, M.; Rovira, C.; Veciana, J.; Klapwijk, T. M.; Aguado, R.; Van Der Zant, H. S. J. Proximity-Induced Shiba States in a Molecular Junction. *Phys. Rev. Lett.* **2017**, *118*, 117001.
(14) Bischoff, F.; Auwärter, W.; Barth, J. V.; Schiffrin, A.; Fuhrer, M.; Weber, B. Nanoscale Phase Engineering of Niobium Diselenide. *Chem. Mater.* **2017**, *29*, 9907−9914.
(15) Komori, F.; Iwaki, T.; Hattori, K.; Shiino, O.; Hasegawa, T. New Superstructure on the Surface of 2H-NbSe2 and Tunneling Spectra at 4.2 K. *J. Phys. Soc. Jpn.* **1997**, *66*, 298−301.
(16) Wang, H.; Lee, J.; Dreyer, M.; Barker, B. I. A scanning tunneling microscopy study of a new superstructure around defects created by tip-sample interaction on 2H- NbSe2. *J. Phys.: Condens. Matter* **2009**, *21*, 265005.
(17) Ara, F.; Qi, Z. K.; Hou, J.; Komeda, T.; Katoh, K.; Yamashita, M. A scanning tunneling microscopy study of the electronic and spin states of bis(phthalocyaninato)terbium(III) (TbPc2) molecules on Ag(111). *Dalton Trans.* **2016**, *45*, 16644−16652.
(18) Katoh, K.; Komeda, T.; Yamashita, M. The Frontier of Molecular Spintronics Based on Multiple-Decker Phthalocyaninato TbIII Single-Molecule Magnets. *Chem. Rec.* **2016**, *16*, 987−1016.
(19) Komeda, T.; Isshiki, H.; Liu, J.; Zhang, Y.-F.; Lorente, N.; Katoh, K.; Breedlove, B. K.; Yamashita, M. Observation and electric current control of a local spin in a single-molecule magnet. *Nat. Commun.* **2011**, *2*, 217.
(20) Takada, M.; Tada, H. Low temperature scanning tunneling microscopy of phthalocyanine multilayers on Au(111) surfaces. *Chem. Phys. Lett.* **2004**, *392*, 265−269.
(21) Chen, L.; Hu, Z. P.; Zhao, A. D.; Wang, B.; Luo, Y.; Yang, J. L.; Hou, J. G. Mechanism for negative differential resistance in molecular electronic devices: Local orbital symmetry matching. *Phys. Rev. Lett.* **2007**, *99*, 146803.
(22) Zhao, A. D.; Hu, Z. P.; Wang, B.; Xiao, X. D.; Yang, J. L.; Hou, J. G. Kondo effect in single cobalt phthalocyanine molecules adsorbed on Au(111) monoatomic steps. *J. Chem. Phys.* **2008**, *128*, 234705.
(23) Hipps, K. W. Copper(II) phthalocyanine: electronic and vibrational tunneling spectra. *J. Phys. Chem.* **1989**, *93*, 5958−5960.
(24) Komeda, T.; Isshiki, H.; Liu, J. Metal-free phthalocyanine (H2Pc) molecule adsorbed on the Au(111) surface: formation of a wide domain along a single lattice direction. *Sci. Technol. Adv. Mater.* **2010**, *11*, 054602.
(25) Ishikawa, N.; Sugita, M.; Ishikawa, T.; Koshihara, S.; Kaizu, Y. Mononuclear lanthanide complexes with a long magnetization relaxation time at high temperatures: A new category of magnets at the single-molecular level. *J. Phys. Chem. B* **2004**, *108*, 11265−11271.
(26) Kondo, J. Resistance Minimum in Dilute Magnetic Alloys. *Prog. Theor. Phys.* **1964**, *32*, 37−49.
(27) Kondo, J. Effect of Ordinary Scattering on Exchange Scattering from Magnetic Impurity in Metals. *Phys. Rev.* **1968**, *169*, 437−440.
(28) Madhavan, V.; Chen, W.; Jamneala, T.; Crommie, M. F.; Wingreen, N. S. Tunneling into a single magnetic atom: Spectroscopic evidence of the Kondo resonance. *Science* **1998**, *280*, 567−569.
(29) Li, J.; Schneider, W. D.; Berndt, R.; Delley, B. Kondo scattering observed at a single magnetic impurity. *Phys. Rev. Lett.* **1998**, *80*, 2893−2896.
(30) Manoharan, H. C.; Lutz, C. P.; Eigler, D. M. Quantum mirages formed by coherent projection of electronic structure. *Nature* **2000**, *403*, 512−515.
(31) Knorr, N.; Schneider, M. A.; Diekhöner, L.; Wahl, P.; Kern, K. Kondo Effect of Single Co Adatoms on Cu Surfaces. *Phys. Rev. Lett.* **2002**, *88*, 096804.
(32) Wahl, P.; Diekhoner, L.; Wittich, G.; Vitali, L.; Schneider, M. A.; Kern, K. Kondo Effect of Molecular Complexes at Surfaces: Ligand Control of the Local Spin Coupling. *Phys. Rev. Lett.* **2005**, *95*, 166601.
(33) Neel, N.; Kroger, J.; Limot, L.; Palotas, K.; Hofer, W. A.; Berndt, R. Conductance and Kondo Effect in a Controlled Single-Atom Contact. *Phys. Rev. Lett.* **2007**, *98*, 016801.
(34) Zhao, A. D.; Li, Q. X.; Chen, L.; Xiang, H. J.; Wang, W. H.; Pan, S.; Wang, B.; Xiao, X. D.; Yang, J. L.; Hou, J. G.; Zhu, Q. S. Controlling the Kondo effect of an adsorbed magnetic ion through its chemical bonding. *Science* **2005**, *309*, 1542−1544.
(35) Hu, Z.; Li, B.; Zhao, A.; Yang, J.; Hou, J. G. Electronic and Magnetic Properties of Metal Phthalocyanines on Au(111) Surface: A First-Principles Study. *J. Phys. Chem. C* **2008**, *112*, 13650−13655.
(36) Gao, L.; Ji, W.; Hu, Y. B.; Cheng, Z. H.; Deng, Z. T.; Liu, Q.; Jiang, N.; Lin, X.; Guo, W.; Du, S. X.; Hofer, W. A.; Xie, X. C.; Gao, H. J. Site-specific Kondo effect at ambient temperatures in iron-based molecules. *Phys. Rev. Lett.* **2007**, *99*, 106402.
(37) Tsukahara, N.; Noto, K. I.; Ohara, M.; Shiraki, S.; Takagi, N.; Takata, Y.; Miyawaki, J.; Taguchi, M.; Chainani, A.; Shin, S.; Kawai, M. Adsorption-Induced Switching of Magnetic Anisotropy in a Single Iron(II) Phthalocyanine Molecule on an Oxidized Cu(110) Surface. *Phys. Rev. Lett.* **2009**, *102*, 167203.
(38) Minamitani, E.; Tsukahara, N.; Matsunaka, D.; Kim, Y.; Takagi, N.; Kawai, M. Symmetry-driven novel Kondo effect in a molecule. *Phys. Rev. Lett.* **2012**, *109*, 086602.
(39) Mugarza, A.; Krull, C.; Robles, R.; Stepanow, S.; Ceballos, G.; Gambardella, P. Spin coupling and relaxation inside molecule-metal contacts. *Nat. Commun.* **2011**, *2*, 490.
(40) Komeda, T.; Isshiki, H.; Liu, J.; Katoh, K.; Shirakata, M.; Breedlove, B. K.; Yamashita, M. Variation of Kondo Peak Observed in the Assembly of Heteroleptic 2,3-Naphthalocyaninato Phthalocyaninato Tb(III) Double-Decker Complex on Au(111). *ACS Nano* **2013**, *7*, 1092−1099.
(41) Iancu, V.; Deshpande, A.; Hla, S. W. Manipulation of the Kondo effect via two-dimensional molecular assembly. *Phys. Rev. Lett.* **2006**, *97*, 266603.
(42) Fernandez-Torrente, I.; Franke, K. J.; Pascual, J. I. Vibrational Kondo Effect in Pure Organic Charge-Transfer Assemblies. *Phys. Rev. Lett.* **2008**, *101*, 217203.

https://doi.org/10.1021/acsnano.1c11221
ACS Nano 2022, 16, 7651−7661

(43) Choi, T.; Bedwani, S.; Rochefort, A.; Chen, C.-Y.; Epstein, A. J.; Gupta, J. A. A Single Molecule Kondo Switch: Multistability of Tetracyanoethylene on Cu(111). *Nano Lett.* **2010**, *10*, 4175−4180.
(44) DiLullo, A.; Chang, S.-H.; Baadji, N.; Clark, K.; Klöckner, J.-P.; Prosenc, M.-H.; Sanvito, S.; Wiesendanger, R.; Hoffmann, G.; Hla, S.-W. Molecular Kondo Chain. *Nano Lett.* **2012**, *12*, 3174−3179.
(45) Warner, B.; El Hallak, F.; Atodiresei, N.; Seibt, P.; Prüser, H.; Caciuc, V.; Waters, M.; Fisher, A. J.; Blügel, S.; Van Slageren, J.; Hirjibehedin, C. F. Sub-molecular modulation of a 4f driven Kondo resonance by surface-induced asymmetry. *Nat. Commun.* **2016**, *7*, 12785.
(46) Barhoumi, R.; Amokrane, A.; Klyatskaya, S.; Boero, M.; Ruben, M.; Bucher, J. P. Screening the 4f-electron spin of TbPc2 single-molecule magnets on metal substrates by ligand channeling. *Nanoscale* **2019**, *11*, 21167−21179.
(47) Komeda, T.; Isshiki, H.; Liu, J.; Katoh, K.; Yamashita, M. Variation of Kondo temperature induced by molecule-substrate decoupling in film formation of bis(phthalocyaninato)terbium(III) molecules on Au(111). *ACS Nano* **2014**, *8*, 4866−4875.
(48) Bauriedl, W.; Ziemann, P.; Buckel, W. Electron-tunneling observation of impurity bands in superconducting manganese-implanted lead. *Phys. Rev. Lett.* **1981**, *47*, 1163−1165.
(49) Balatsky, A. V.; Vekhter, I.; Zhu, J. X. Impurity-induced states in conventional and unconventional superconductors. *Rev. Mod. Phys.* **2006**, *78*, 373−433.
(50) Flatté, M. E.; Byers, J. M. Local Electronic Structure of a Single Magnetic Impurity in a Superconductor. *Phys. Rev. Lett.* **1997**, *78*, 3761−3764.
(51) Choi, D. J.; Fernández, C. G.; Herrera, E.; Rubio-Verdú, C.; Ugeda, M. M.; Guillamón, I.; Suderow, H.; Pascual, J. I.; Lorente, N. Influence of Magnetic Ordering between Cr Adatoms on the Yu-Shiba-Rusinov States of the β-Bi2Pd Superconductor. *Phys. Rev. Lett.* **2018**, *120*, 167001.
(52) Franke, K. J.; Schulze, G.; Pascual, J. I. Competition of superconducting phenomena and Kondo screening at the nanoscale. *Science* **2011**, *332*, 940−944.
(53) Liebhaber, E.; Acero González, S.; Baba, R.; Reecht, G.; Heinrich, B. W.; Rohlf, S.; Rossnagel, K.; Von Oppen, F.; Franke, K. J. Yu-Shiba-Rusinov States in the Charge-Density Modulated Superconductor NbSe2. *Nano Lett.* **2020**, *20*, 339−344.
(54) Farinacci, L.; Ahmadi, G.; Reecht, G.; Ruby, M.; Bogdanoff, N.; Peters, O.; Heinrich, B. W.; Von Oppen, F.; Franke, K. J. Tuning the Coupling of an Individual Magnetic Impurity to a Superconductor: Quantum Phase Transition and Transport. *Phys. Rev. Lett.* **2018**, *121*, 196803.
(55) Farinacci, L.; Ahmadi, G.; Ruby, M.; Reecht, G.; Heinrich, B. W.; Czekelius, C.; Von Oppen, F.; Franke, K. J. Interfering Tunneling Paths through Magnetic Molecules on Superconductors: Asymmetries of Kondo and Yu-Shiba-Rusinov Resonances. *Phys. Rev. Lett.* **2020**, *125*, 256805.
(56) Huang, H.; Drost, R.; Senkpiel, J.; Padurariu, C.; Kubala, B.; Yeyati, A. L.; Cuevas, J. C.; Ankerhold, J.; Kern, K.; Ast, C. R. Quantum phase transitions and the role of impurity-substrate hybridization in Yu-Shiba-Rusinov states. *Commun. Phys.* **2020**, *3*, 199.
(57) Kezilebieke, S.; Dvorak, M.; Ojanen, T.; Liljeroth, P. Coupled Yu−Shiba−Rusinov States in Molecular Dimers on NbSe2. *Nano Lett.* **2018**, *18*, 2311−2315.
(58) Kezilebieke, S.; Žitko, R.; Dvorak, M.; Ojanen, T.; Liljeroth, P. Observation of Coexistence of Yu-Shiba-Rusinov States and Spin-Flip Excitations. *Nano Lett.* **2019**, *19*, 4614−4619.
(59) Rubio-Verdú, C.; Zaldívar, J.; Žitko, R.; Pascual, J. I. Coupled Yu-Shiba-Rusinov States Induced by a Many-Body Molecular Spin on a Superconductor. *Phys. Rev. Lett.* **2021**, *126*, 017001.
(60) Salkola, M. I.; Balatsky, A. V.; Schrieffer, J. R. Spectral properties of quasiparticle excitations induced by magnetic moments in superconductors. *Phys. Rev. B* **1997**, *55*, 12648−12661.
(61) Wang, Y.; Arabi, S.; Kern, K.; Ternes, M. Symmetry mediated tunable molecular magnetism on a 2D material. *Commun. Phys.* **2021**, *4*, 103.
(62) Adler, H.; Paszkiewicz, M.; Uihlein, J.; Polek, M.; Ovsyannikov, R.; Basova, T. V.; Chassé, T.; Peisert, H. Interface properties of VOPc on Ni(111) and graphene/Ni(111): Orientation-dependent charge transfer. *J. Phys. Chem. C* **2015**, *119*, 8755−8762.
(63) Niu, T.; Zhang, J.; Chen, W. Molecular ordering and dipole alignment of vanadyl phthalocyanine monolayer on metals: The effects of interfacial interactions. *J. Phys. Chem. C* **2014**, *118*, 4151−4159.
(64) Blowey, P. J.; Maurer, R. J.; Rochford, L. A.; Duncan, D. A.; Kang, J. H.; Warr, D. A.; Ramadan, A. J.; Lee, T. L.; Thakur, P. K.; Costantini, G.; Reuter, K.; Woodruff, D. P. The Structure of VOPc on Cu(111): Does V═O Point Up, or Down, or Both? *J. Phys. Chem. C* **2019**, *123*, 8101−8111.
(65) Fernández, L.; Thussing, S.; Mänz, A.; Witte, G.; Brion-Rios, A. X.; Cabrera-Sanfelix, P.; Sanchez-Portal, D.; Jakob, P. Structural and Vibrational Properties of the TiOPc Monolayer on Ag(111). *J. Phys. Chem. C* **2017**, *121*, 1608−1617.
(66) Wang, Y.; Kröger, J.; Berndt, R.; Hofer, W. Structural and Electronic Properties of Ultrathin Tin−Phthalocyanine Films on Ag(111) at the Single-Molecule Level. *Angew. Chem., Int. Ed.* **2009**, *48*, 1261−1265.
(67) Niu, T.; Zhou, M.; Zhang, J.; Feng, Y.; Chen, W. Dipole Orientation Dependent Symmetry Reduction of Chloroaluminum Phthalocyanine on Cu(111). *J. Phys. Chem. C* **2013**, *117*, 1013−1019.
(68) Qin, D.; Ge, X.-J.; Lü, J.-T. Tin-phthalocyanine adsorption and diffusion on Cu and Au (111) surfaces: A density functional theory study. *Surf. Sci.* **2018**, *671*, 6−10.
(69) Schwarz, F.; Wang, Y. F.; Hofer, W. A.; Berndt, R.; Runge, E.; Kröger, J. Electronic and Vibrational States of Single Tin−Phthalocyanine Molecules in Double Layers on Ag(111). *J. Phys. Chem. C* **2015**, *119*, 15716−15722.
(70) Sperl, A.; Kröger, J.; Berndt, R. Demetalation of a Single Organometallic Complex. *J. Am. Chem. Soc.* **2011**, *133*, 11007−11009.
(71) Bocquet, M.-L.; Lesnard, H.; Monturet, S.; Lorente, N. Theory of Elastic and Inelastic Electron Tunneling. *Computational Methods in Catalysis and Materials Science* **2009**, 199.
(72) Tersoff, J.; Hamann, D. R. Theory and Application for the Scanning Tunneling Microscope. *Phys. Rev. Lett.* **1983**, *50*, 1998−2001.
(73) Komeda, T.; Okabayashi, N. Spatially Resolved Surface Vibrational Spectroscopies. *Springer Handbook of Surface Science* **2020**, 815.
(74) Stipe, B. C.; Rezaei, M. A.; Ho, W. Single-molecule vibrational spectroscopy and microscopy. *Science* **1998**, *280*, 1732−1735.
(75) Franke, K. J.; Schulze, G.; Pascual, J. I. Excitation of Jahn-Teller active modes during electron transport through single C60 molecules on metal surfaces. *J. Phys. Chem. Lett.* **2010**, *1*, 500−504.
(76) Heinrich, B. W.; Braun, L.; Pascual, J. I.; Franke, K. J. Protection of excited spin states by a superconducting energy gap. *Nat. Phys.* **2013**, *9*, 765−768.
(77) Burgess, J. A. J.; Malavolti, L.; Lanzilotto, V.; Mannini, M.; Yan, S.; Ninova, S.; Totti, F.; Rolf-Pissarczyk, S.; Cornia, A.; Sessoli, R.; Loth, S. Magnetic fingerprint of individual Fe4 molecular magnets under compression by a scanning tunnelling microscope. *Nat. Commun.* **2015**, *6*, 8216.
(78) Mier, C.; Verlhac, B.; Garnier, L.; Robles, R.; Limot, L.; Lorente, N.; Choi, D.-J. Superconducting Scanning Tunneling Microscope Tip to Reveal Sub-millielectronvolt Magnetic Energy Variations on Surfaces. *J. Phys. Chem. Lett.* **2021**, *12*, 2983−2989.
(79) Ishikawa, N.; Sugita, M.; Wernsdorfer, W. Quantum tunneling of magnetization in lanthanide single-molecule magnets: Bis(phthalocyaninato)terbium and bis(phthalocyaninato)dysprosium anions. *Angew. Chem., Int. Ed.* **2005**, *44*, 2931−2935.
(80) Sarwar, S.; Sanz, S.; Van Leusen, J.; Nichol, G. S.; Brechin, E. K.; Kögerler, P. Phthalocyanine-polyoxotungstate lanthanide double deckers. *Dalton Trans.* **2020**, *49*, 16638−16642.

https://doi.org/10.1021/acsnano.1c11221
ACS Nano 2022, 16, 7651−7661

(81) Pederson, R.; Wysocki, A. L.; Mayhall, N.; Park, K. Multireference Ab Initio Studies of Magnetic Properties of Terbium-Based Single-Molecule Magnets. *J. Phys. Chem. A* **2019**, *123*, 6996−7006.
(82) Huang, H.; Van den Heuvel, W.; Soncini, A. Lanthanide-Radical Magnetic Coupling in [LnPc2]0: Competing Exchange Mechanisms Captured via Ab Initio Multi-Reference Calculations. *Quantum Mater. Res.* **2020**, *1*, e200003.
(83) Boukhvalov, D. W.; Dobrovitski, V. V.; Kögerler, P.; Al-Saqer, M.; Katsnelson, M. I.; Lichtenstein, A. I.; Harmon, B. N. Effect of ligand substitution on the exchange interactions in {Mn 12}-type single-molecule magnets. *Inorg. Chem.* **2010**, *49*, 10902−10906.
(84) Kresse, G.; Furthmuller, J. Efficiency of ab-initio total energy calculations for metals and semiconductors using a plane-wave basis set. *Comput. Mater. Sci.* **1996**, *6*, 15−50.
(85) Kresse, G.; Joubert, D. From ultrasoft pseudopotentials to the projector augmented-wave method. *Phys. Rev. B* **1999**, *59*, 1758−1775.
(86) Perdew, J. P.; Burke, K.; Ernzerhof, M. Generalized gradient approximation made simple. *Phys. Rev. Lett.* **1996**, *77*, 3865−3868.
(87) Momma, K.; Izumi, F. VESTA 3 for Three-Dimensional Visualization of Crystal, Volumetric and Morphology Data. *J. Appl. Crystallogr.* **2011**, *44*, 1272−1276.

https://doi.org/10.1021/acsnano.1c11221
ACS Nano 2022, 16, 7651−7661